

## The Day/Night Visible Sensor Aboard NPOESS VIIRS

Thomas F. Lee\*  
Steven D. Miller  
F. Joseph Turk  
Naval Research Laboratory, Monterey California

Carl Schueler  
Richard Julian  
Raytheon Corporation, Santa Barbara California

Chris Elvidge  
National Geophysical Data Center  
Boulder Colorado

Steve Deyo  
Patrick Dills  
Sherwood Wang  
UCAR/COMET  
Boulder Colorado

### 1. Introduction

The Visible/Infrared Imager/Radiometer Suite (VIIRS) is the next generation visible and infrared sensor slated to fly on the National Polar-orbiting Operational Environmental Satellite System (NPOESS) and NPOESS Preparatory Satellite (NPP) platforms. The twenty-two channels featured on VIIRS are derived primarily from two legacy instruments: the NOAA Advanced Very High Resolution Radiometer (AVHRR) and Earth Observation System (EOS) Moderate Resolution Imaging Spectroradiometer (MODIS). The lone exception is the VIIRS Day/Night band (hereafter, DNB), which draws heritage from the low-light nighttime visible sensing capability upon the Defense Meteorological Satellite Program (DMSP) Operational Linescan System (OLS) instrument. In this way, VIIRS assembles the best capabilities of contemporary operational and research observing systems for tomorrow's operational constellation.

The DNB will measure visible radiances from the earth and atmosphere (both natural and anthropogenic nighttime light emissions) during both day and night portions of the orbit. To achieve satisfactory radiometric resolution across the immense dynamic range (seven orders of magnitude) encountered over a single orbit, the DNB selects its gain dynamically from three simultaneously collecting stages residing upon the same focal plane array. In comparison to the OLS, some of the VIIRS DNB channel improvements include 1) reduced instances of pixel saturation, 2) smaller instantaneous field of view (IFOV, leading to reduced spatial blurring), 3) superior calibration and radiometric resolution, 4) co-location with multispectral measurements upon VIIRS and other NPOESS sensors, 5) and generally increased spatial resolution with effective elimination of cross-track pixel size variation.

This paper sets out first to provide an overarching description of the DMSP-OLS and VIIRS-DNB sensors, comparing and contrasting their engineering designs. It will then discuss, in the context of nighttime imagery examples as provided from the OLS, both the current capabilities and anticipated improvements afforded by the

---

\*Corresponding author address: Thomas F. Lee, Naval Research Laboratory, Monterey, CA 93943-5502; e-mail: [lee@nrlmry.navy.mil](mailto:lee@nrlmry.navy.mil)

VIIRS DNB. Specifically, the paper treats the following topics: 1) lunar reflection in the context of cloud, dust, smoke and snow/ice detection and analysis, 2) visible emissions in the context of lightning, fire, aurora, and anthropogenic sources, and 3) user training for optimizing utility and minimizing interpretive pitfalls of this unique dataset. The paper concludes with a discussion of how additional VIIRS channels will provide through synergy a variety of new environmental products not available to the current OLS nighttime visible channel.

## 2. DMSP OLS Overview

The DMSP-OLS (Johnson et al 1994; Elvidge *et al.* 1997, Elvidge *et al.* 1998b) has been operated by the United States Air Force since the late 1960's, but declassified images only became available in 1973 (Croft 1978). The primary mission of the OLS was to monitor cloud cover. In particular, the purpose of the nighttime visible was to extend the daytime capability to moonlit conditions. The capability bore particular relevance to clouds that were inherently difficult to detect from infrared imagery due to lack of thermal contrast with the surface (e.g., low clouds and fog). The first USAF meteorologists who laid eyes on OLS nighttime visible images were amazed to see collections of bright spots on the images corresponding to locations of known cities. These city lights were particularly prominent under higher gain settings (applied in conditions of little or no moon) but could be seen less well under in lower gain settings (full moon). The cities could often be seen through cloud structures, though their shapes would sometimes be distorted (Croft 1978). Only the thickest clouds were capable of completely attenuating the light of major cities.

The instrument consists of three instruments: telescopes for the visible and infrared bands and a photomultiplier tube for the day/night band, imaged in 3000 km swaths. The visible channel actually covers both the visible and near-infrared portion of the spectrum (Elvidge et al. 1998a). The visible data are partitioned into only 64 levels of gray. While the lack of spectral and radiometric resolution available on OLS

hampers its extension to other quantitative environmental applications, the instrument meets adequately the requirements for the task for which it was designed. The infrared channel has 256 levels of gray. At night the visible signal is enhanced by using a photomultiplier tube, making it possible to detect low emissions. It can detect lights, fires, and gas flares. With sufficient moonlight snow cover, sea ice, clouds, and land surface features can be detected. There are two main spatial resolutions, a smooth mode at 2.7 km and a fine mode at .56 km. Only one of the two channels can be "fine" at once. If the visible is fine, then infrared is smooth to save transmission bandwidth. If the infrared is fine, then the visible is smooth. Central Air Force planners decide which channel is smooth and which is fine. This is programmable depending on location and season.

The spatial resolution figures listed above overstate the ability of the sensor to produce effective visible images at night. This discrepancy occurs because the effective instantaneous field of view (EIFOV) of the nighttime sensor is much larger than the nominal footprint size, leading to substantial pixel overlap. Fortunately, the OLS technology employs a number of strategies to restrain the EIFOV as a function of scan angle. The EIFOV ranges from 2.2 km at subpoint to 4.2 km at 766 km out from the nadir. Then after a switch in aperture, the EIFOV is reduced to 3.0 km, rising to 5.4 km at the edge of scan (Elvidge 1998b). The large, overlapping EIFOV's greatly limit the sharpness and detail of DMSP-OLS nighttime images.

The OLS nighttime band is designed to handle an enormous range of cloud illumination. At the high end of illumination range, the sensor measures reflected solar radiance at the day/night terminator. At a lower level it is able to detect clouds based on the radiation provided by a full moon high in the night sky. At the lowest level it detects clouds illuminated by partial moon, or a moon low in the night sky. Also, clouds are not seen when the moon, whatever the phase, is below the horizon. To accommodate for this large range of illumination, an automatic gain is applied to normalize the data for viewing. It is

important to realize that the early design anticipated that the data would be imaged for forecasting applications, not used in a quantified way, e.g., in scientific algorithms. Thus, though the gain normalizes the appearance of images under different lighting regimes, it makes digital use of the data very difficult.

To date, the OLS nighttime visible band has been one of most poorly exploited of operational sensors aboard environmental satellites. There have been several reasons for this. First, realtime OLS data has been restricted to U.S. Department of Defense customers in real time, and until only recently has been exceedingly difficult to obtain from the archives. The National Geophysical Data Center (NGDC) has made begun making available the global data from the last decade. Second, uncalibrated, six-bit (64 gray shades) visible digital data has precluded use in high fidelity products. Third, since the OLS is a bi-spectral imager, the scope of environmental applications is considerably limited. The division of data into fine (high resolution) and smooth (low resolution) categories has further complicated interpretation of various DMSP products.

### **3. NPOESS VIIRS DNB Overview**

The NPOESS Visible Infrared Imager/Radiometer Suite (VIIRS) Day/Night Band (DNB) sensor is implemented as a dedicated Focal Plane Assembly (FPA) and associated electronics in the VIIRS sensor, sharing the optics and scan mechanism with the other VIIRS spectral bands. This integral design approach offers lower overall VIIRS complexity, cost, mass, and volume compared to a separate DNB sensor. It also offers DNB radiometric calibration with accuracy comparable to the other VIIRS spectral bands.

Every 1.786 seconds as NPOESS VIIRS orbits the earth in a near-polar "terminator" orbit, the DNB sensor will scan an 11.87 km (along track) by 3109 km (cross track) swath of earth scene across the terminator, 16 pixels along track by 4,064 pixels cross track. Moreover, although there is no requirement for DNB data samples to overlay samples from other VIIRS spectral bands, the fact that the DNB optics and scan are common with all other VIIRS spectral bands allows the relative location of pixels from all bands to be accurately known. The geographic locations of DNB pixels relative to other VIIRS bands are expected to be known within about 30 meters even at the edge of scan (EOS). Table 1 lists the most important VIIRS DNB sensor performance parameters.

Table 1: Key VIIRS DNB sensor performance characteristics

Description	Value	Units
Spectral Passband Center	0.7	μm
Spectral Bandwidth	0.4	μm
Horizontal Sample Interval, Track & Scan Directions (Applies across full earth scan)	742 +/- 5%	meters
SNR At minimum scene radiance - End of Scan	6	
SNR At minimum scene radiance - nadir	30	
Minimum scene radiance (within spectrum 0.4-1.0 micron)	4.0E-05	W/m <sup>2</sup> -sr
Minimum Saturation radiance (wavelength range 0.4-1 micron)	500	W/m <sup>2</sup> -sr
A/D Conversion Quantization - Lowest Radiance Stage	14	bits
A/D Conversion Quantization - Med & High Radiance Stages	13	bits
Calibration Uncertainty:		
High-Gain Stages At Lmin for stage & at Lmax for stage	100%, 30%	%
Med-Gain Stage At L min for stage, & at Lmax for stage	30%, 10%	%
Low-Gain Stage At L min for stage, & at 0.5 x Lmax for stage	10%, 5%	%

A/D – Analog to Digital Converter

Lmin & Lmax – minimum & maximum expected radiances

DNB image detection is performed by a versatile, multistage Charge-Coupled Device (CCD) on the FPA. CCDs offer many benefits in the DNB sensor application, including dynamic range up to 1,000 from a single detector, essentially-noiseless Time Delay Integration (TDI) and signal aggregation, and a near-perfect (unity) “drag” component of modulation transfer function (MTF). The DNB CCD FPA incorporates separate stages (groups of detectors) to detect low, medium, and high-radiance scenes, with relative radiometric gains of 119,000:477:1 (high:medium:low gain). Two identical copies of the high-gain stage are provided, which improves signal-to-noise ratio (SNR) at low radiances and allows correction of pixels impacted by high-energy subatomic particles.

The scene is scanned sequentially across these four gain stages so that each pixel on the ground is imaged with all three gains in less than 3 msec time difference from high to low gain for a given point on the earth. The signals from all stages are then digitized, and logic in the VIIRS Electronics Module (EM) subsequently selects, on an individual pixel basis, which of the three digital values should be transmitted to earth. In general, the VIIRS EM logic chooses the

most sensitive stage in which the pixel is not saturated.

The use of multiple detector stages followed by data selection means that each pixel retains the full DNB dynamic range, so that bright pixels against dark night scenes will not saturate in DNB data. The data set is ideally suited to produce “constant contrast” imagery, in which the pixel data are converted into radiance units and these are then divided by the radiance illuminating each pixel to yield a measure of the pixel’s scene reflectance. The desired result is that the entire scene will appear as if it were uniformly illuminated. The distracting effects of non-uniform illumination will be eliminated even from terminator scenes, which can extend in a single scan from darkest night on one side to daylight on the other side.

The sensitive area of each CCD stage is divided into subpixels, each smaller than the area needed to image a full DNB scene pixel. The CCD aggregates the signals from groups of these “subpixel” detectors in both the along-track and cross-track directions to create an “effective detector” with constant geometric instantaneous field of view (GIFOV) on the ground by varying the angular instantaneous field of view (IFOV). The angular IFOV is relatively large at nadir,

and narrower at EOS so that the projected ground "footprint" on the earth will be essentially constant both along and cross track at 742 meters (with a tolerance of  $\pm 5\%$ ) over the entire swath. Because the ground footprints of all other VIIRS spectral bands grow by 2.1x along track and 6.1x cross-track from nadir to EOS, the DNB pixels do not generally "nest" with pixels from other bands. "Nesting" is desirable for multi-spectral applications of different resolution bands, and the other VIIRS spectral bands with different spatial resolution do mutually "nest." The lack of a co-registration requirement between DNB and the other VIIRS bands, however, coupled with the importance of a DNB product with near-constant contrast and resolution, led to a design tradeoff making "nesting" impractical between DNB and the other VIIRS spectral bands.

The narrower angular IFOV at EOS results in collection of fewer photons and thus lower SNR at EOS compared to elsewhere in the scan. As shown in Table 1, the DNB still meets SNR requirements at EOS and offers substantial SNR margin over most of the swath even under the lowest light conditions. The aggregation - and thus the SNR - changes at 32 discrete "aggregation mode" switching-points between nadir and EOS on either side of nadir. The radiometric gain of each DNB stage therefore has 32 different levels during the scan, proportional to the number of subpixels aggregated in each of the 32 discrete aggregation modes. Specifically, 12.6x more subpixels are aggregated at nadir than at EOS, so that the saturation radiance of each gain stage is 12.6x greater at EOS than at nadir, while the SNR is about 3.4x higher at nadir than at EOS. Moreover, both CCD detection and aggregation are near-linear over the full DNB dynamic range. This enables an effective on-orbit radiometric calibration of DNB imagery to accuracies significantly better than the OLS specification, despite the absence of calibration targets with known radiances in the middle and low-radiance ranges of the DNB.

## 4. Lunar Reflection-Based Applications

### *Lunar Cycle Considerations:*

The amount of solar illumination reflected off the moon and available to illuminate clouds and the surface of the earth depends on lunar phase and lunar elevation in the sky. The amount of lunar illumination provided by the moon is not linear as a function of the portion of the moon that is lit. This is due to the fact that shadows produced by craters, ridges, etc. are minimized at full moon which resembles midday. The intensity of illumination is about nine times greater at full moon than at the first or third quarter moon. Perhaps surprisingly, the moon is not an efficient reflector of solar energy with an albedo of about 0.07 vs. 0.39 for the earth.

There are a variety of factors that influence the path of the moon around the earth, complicating the understanding of its orbit (Foster and Hall 1991). The full moon is low in the sky in summer, but in winter the full moon is much higher in the sky. This configuration follows from the fact that the full moon is always opposite the sun in the sky. In winter at  $45^\circ$  N the midday sun is about  $22^\circ$  above the southern horizon, but the midnight full moon is about  $68^\circ$  above the southern horizon on average. Thus, the lunar illumination is strongest in exactly the season when solar illumination is the weakest. Thus, nighttime visible imaging has a powerful niche in wintertime. Moreover, uneven illumination and shadows, problems which plague winter imaging of snow and ice during the daytime using visible wavelengths, are often greatly reduced in nighttime visible images.

The latitudinal oscillation of the sun about the equator follows an annual cycle. In a similar way, latitudinal motions of the moon follow a cycle on a monthly time scale. Thus, in a period of just a few nights the elevation of the moon can change significantly. This means that the illumination over even unchanging terrestrial features will change significantly in a short period of time, and the positions of shadows and other terrain-induced variations of illumination will also change. In the Arctic and Antarctic nights, the moon will be above the horizon at all times during a twenty-four hour period at

high latitudes (corresponding to the sun being always below the horizon in the season), allowing useful images based on

overpasses which are frequent near the poles.

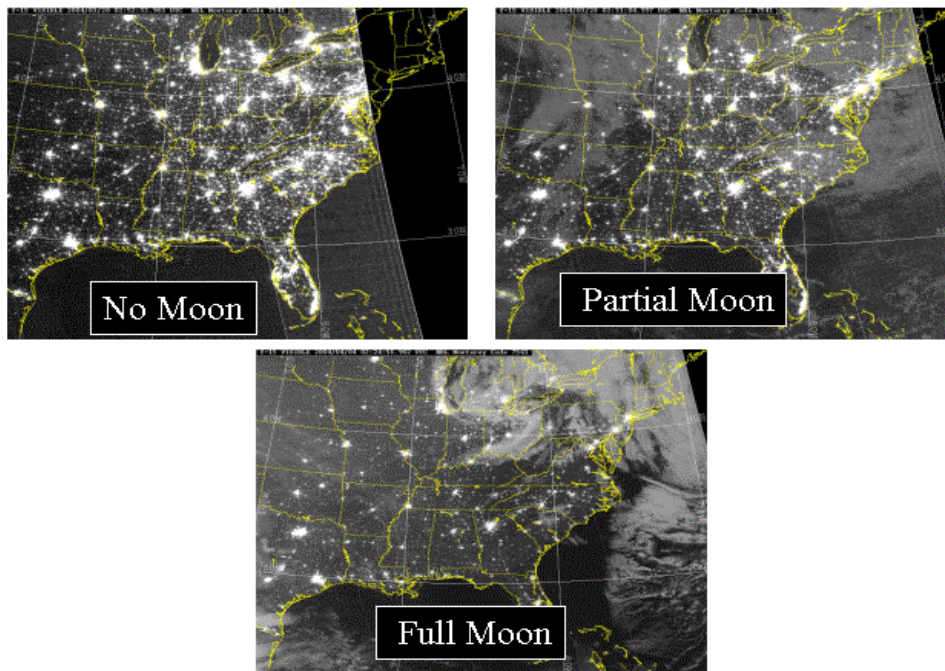


Fig. 1 Three DMSP-OLS (F-15) nighttime visible scenes during March/April 2004.

#### ***Cloud Detection as a Function of Lunar Phase:***

Fig. 1 shows cloud the ability of the DMSP-OLS to detect clouds under three different levels of lunar illumination. All three of the scenes contain clouds, but only the “partial moon” and “full moon” images have sufficient lunar illumination to show them. It is easy but incorrect to believe that the “no moon” case is cloud free since cities can be easily seen everywhere. In fact, there are un-illuminated clouds in the scene; however, they are sufficiently thin to allow the city lights to be seen through them. Within the “partial moon” scene, limited illumination allows clouds to be seen, but they lack crispness. Cities can be seen through many of the clouds. In the bottom image (full moon) robust lunar illumination allows clouds to be seen in detail. Notice that with reduced gain fewer cities are seen here than in the “no moon” image that was produced under high gain.

#### ***Dust and Smoke Detection:***

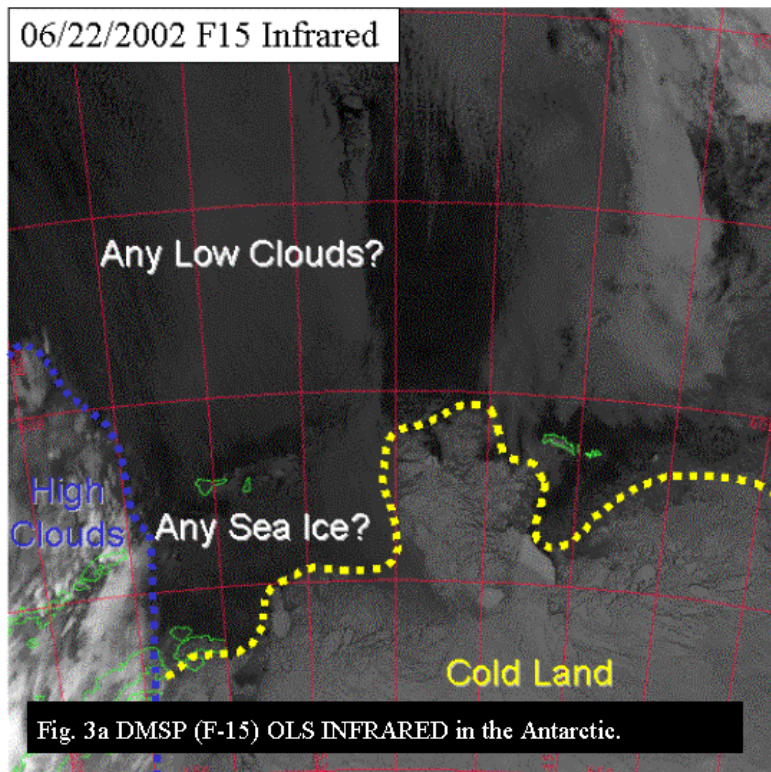
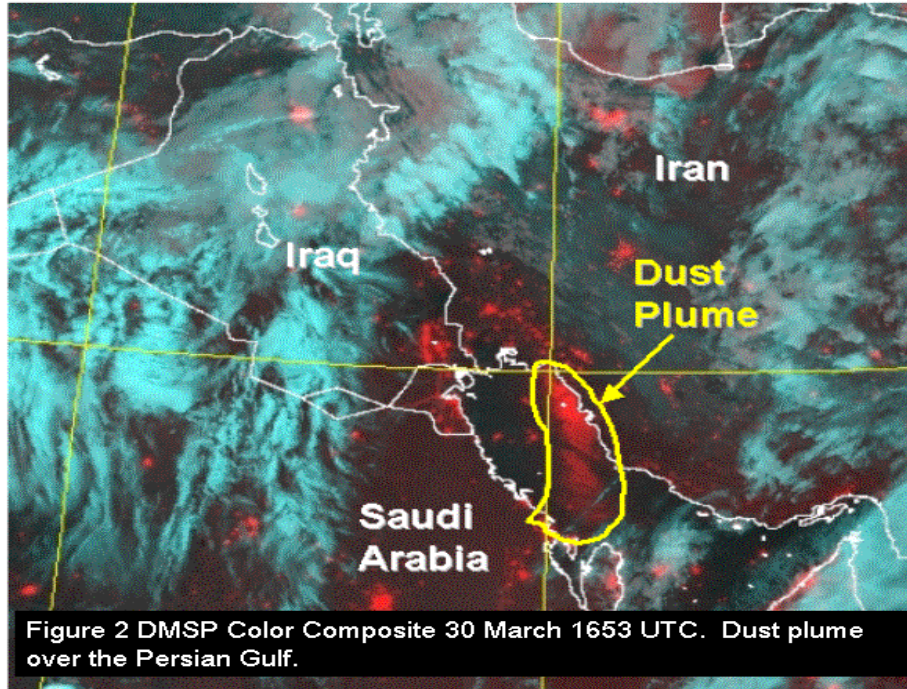
The DMSP-OLS can view blowing and suspended dust in a similar way that clouds can be viewed. First, there needs to be sufficient lunar illumination, and second, the dust needs to be thick enough to be imaged. Over land areas, visible images are limited even during the daytime because of lack of contrast between airborne dust and the background. At night this same difficulty applies. To assist in dust detection, we constructed a bispectral composite. The nighttime visible under moonlit conditions is put into the red gun; the infrared is placed into the blue and green guns. This allows for better depiction of clouds. High clouds show up blue; low clouds and blowing dust show as red. Fig. 2 shows a plume of dust moving south over the Persian Gulf region.

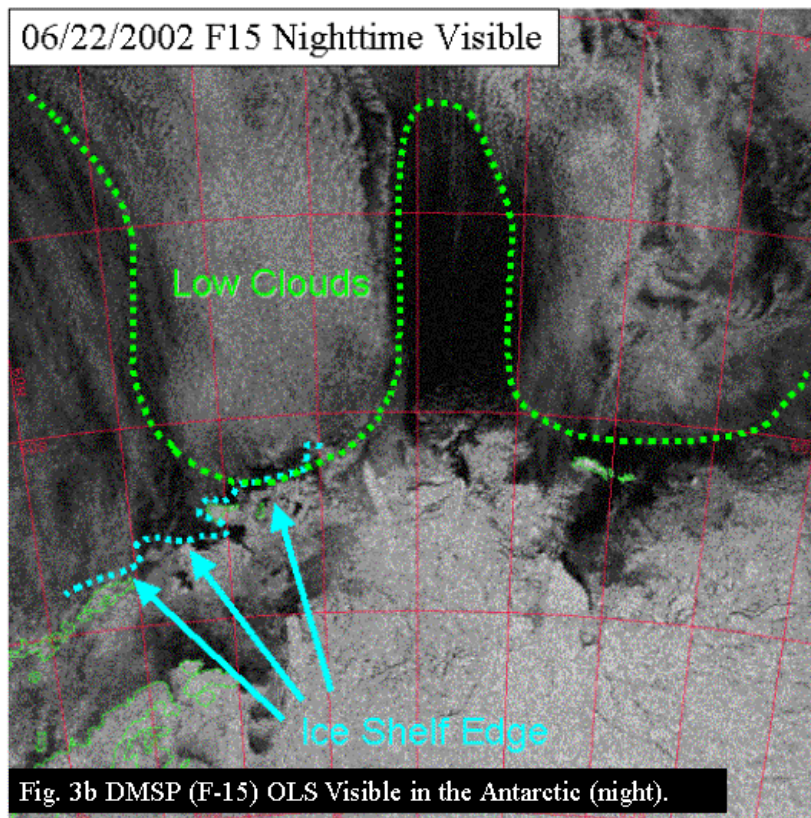
#### ***Snow and Ice:***

At present visible satellite sensors remain one of the viable means to observe and map snow and ice cover. The problem with visible sensing is that most sensors only

have the capacity for daytime measurements. The daytime restriction severely limits observation during winter when nights are long. This season matches the time of the most need for accurate snow cover observations in many regions. Of course, this problem becomes extreme near

the poles where Arctic (Antarctic) night prevails during the winter. Infrared and passive microwave sensors also have capability to observe snow but have several limitations. Infrared sensors, and especially passive microwave imagers, often lack the





high spatial resolution of visible sensors. Even high-resolution infrared sensors often produce featureless images because of the lack of thermal contrast inherent in many winter scenes. Infrared images often cannot be used even to distinguish regions of snow from adjacent snow-free areas. Thus, the nighttime visible image is an important tool for this application (Foster 1983; Foster and Hall 1991).

Fig. 3a shows a DMSP OLS fine resolution infrared image over coastal Antarctica during the winter dark season. The ice edge can be seen just south of 60° S, but it is indistinct due to clouds that have similar gray shades. In fact, in this case the low clouds (annotated) are even darker (warmer) than the ice below. To the west of the low cloud area, high clouds obscure island and ice features. Under a full moon the nighttime visible shows the ice edge in greater detail (Fig. 3b). Both high and low clouds are often thin in the Antarctic, allowing a view of the ice and island features beneath the clouds. Fig. 3b image is low spatial resolution (2.7 km). The “grainy” appearance is produced because only 64

levels of brightness are conveyed in the data sets. Therefore further image enhancement, possible using other sensors like the NOAA AVHRR, is impossible. In the NPOESS VIIRS era, this will all change. More display gray shades (roughly 4096), the availability of other multispectral measurements, and smaller fields of view will combine to produce much better imagery and opportunities for quantitative applications.

## 5. Emission-Based Applications

### *Anthropogenic Sources: City Lights and Natural Gas Flares*

Much of the published research on the nighttime DMSP-OLS nighttime visible channels visible has focused on the mapping of artificial lights on the surface of earth, especially from cities (Sullivan 1989; Elvidge et al 1997, Elvidge et al 1998b). The ability to see lights is greatest in periods without moon as in Fig. 4, a false color composite of the Persian Gulf region. It is similar to Fig. 2 but has a somewhat

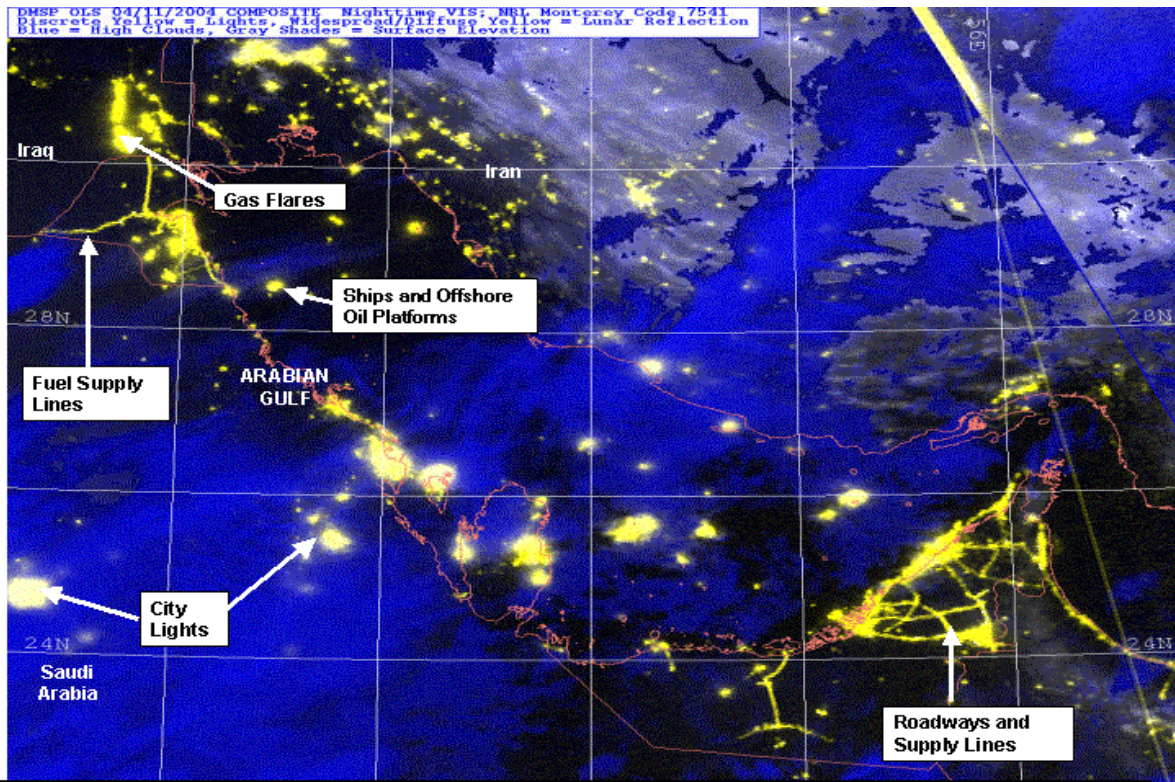


Fig. 4 DMSP OLS Nighttime Visible, 11 April 2004. Color composite of several bands.

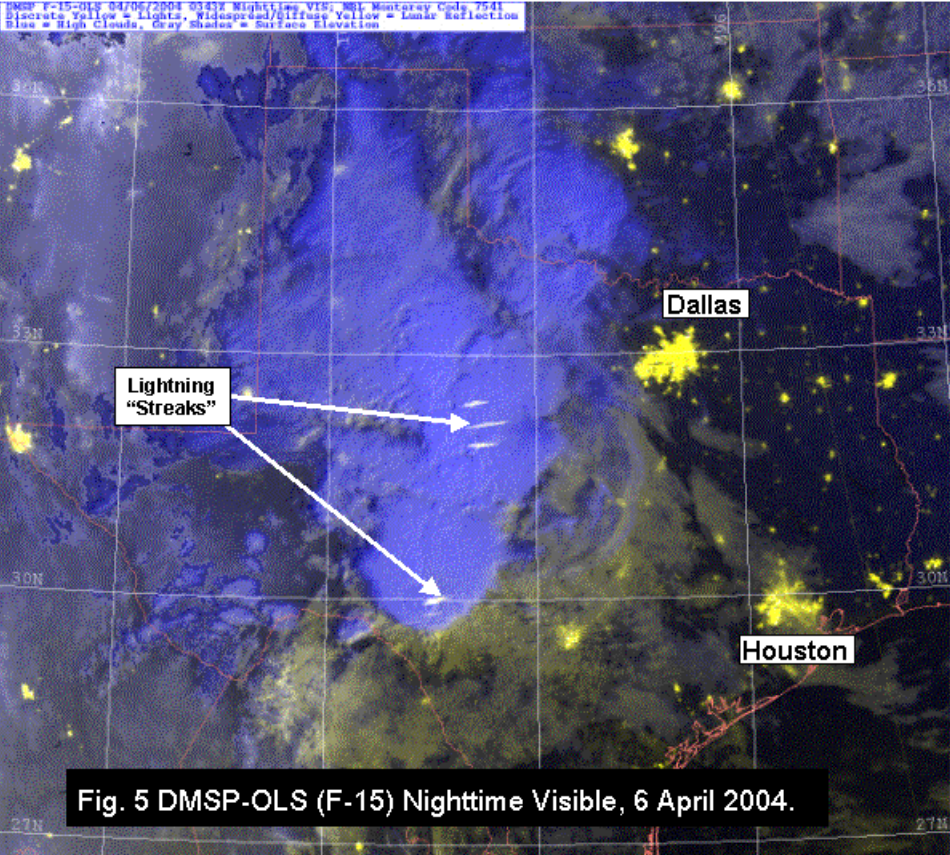


Fig. 5 DMSP-OLS (F-15) Nighttime Visible, 6 April 2004.

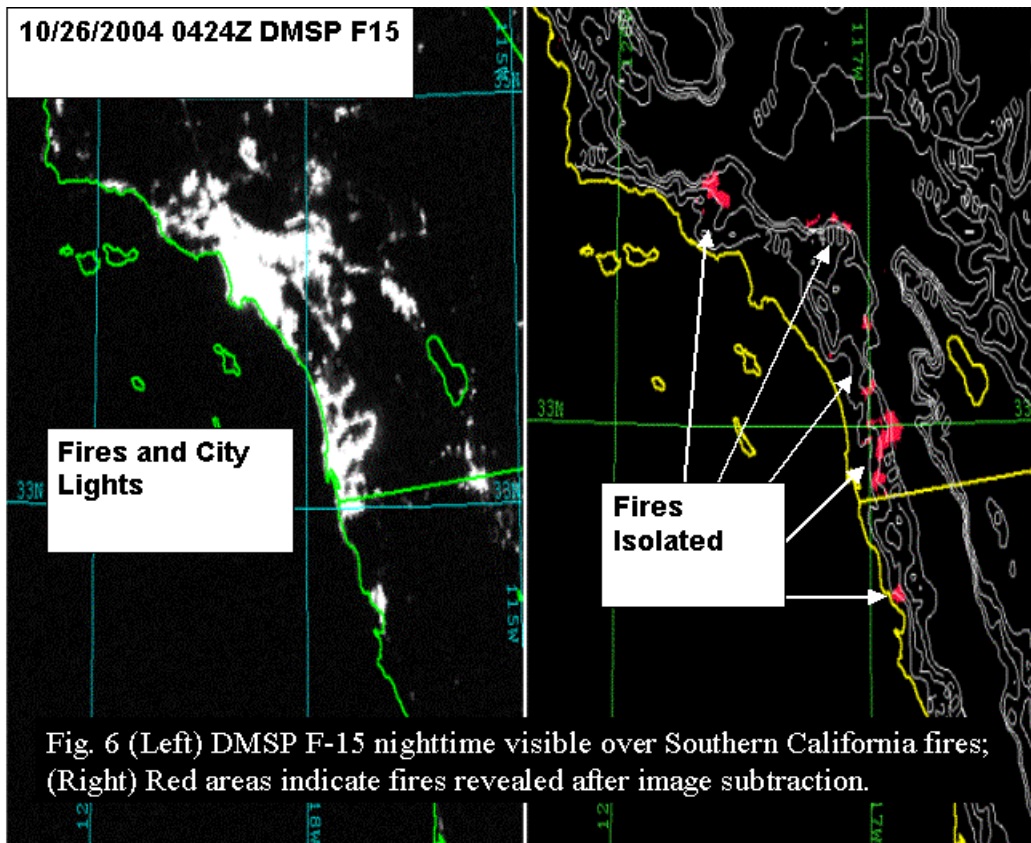


Fig. 6 (Left) DMSP F-15 nighttime visible over Southern California fires; (Right) Red areas indicate fires revealed after image subtraction.

different color scheme. Lights and roads are yellow; clouds are blue.

**Atmospheric Sources: Lightning and Auroras**

Fig. 5 shows a nighttime visible color composite over Texas. The streaks may appear to be noise, but are actually lightning (Orville 1981; Orville and Henderson 1986). High clouds are blue; cities are yellow, and low clouds (illuminated under moonlight) are also yellow.

**Wildfire Detection: The Southern California Fires of Fall, 2004**

Both DMSP OLS and NOAA AVHRR have proven capability in fire detection (Elvidge et al. 1997; Elvidge et al. 1996; Fuller and Fulk 2000). Fires can be detected from the OLS at night based on the identification of lights known not to be from non-lights sources (Elvidge et al 1998). Based on NOAA AVHRR, fires can be detected from multispectral radiances, especially based on the 3.7  $\mu\text{m}$  (shortwave infrared) channel. VIIRS will have the great advantage of having both the shortwave infrared and the

day/night band on the same platform, plus twenty additional channels. Thus, both visible/near-infrared light and thermal radiances will be able to confirm the existence of fires and estimate their size.

Fig. 6 (left side) shows a DMSP nighttime visible image over southern California during the devastating wild fires in the fall of 2003. No smoke plumes appear because of the lack of moonlight during this period. While fires are visible in this image as light sources, it is nearly impossible to distinguish them from background lights from city lights. To isolate the fire signatures, we create a pixel-by-pixel difference image of this image with a similar image a few days earlier prior to the onset of fires. The differencing technique cancels the non-fire lights, leaving only the fires. (Fig. 6 right).

**6. User Training for the DNB**

One of the main barriers to more use of the nighttime OLS images, even within the Department of Defense, has been lack of understanding by the end users.

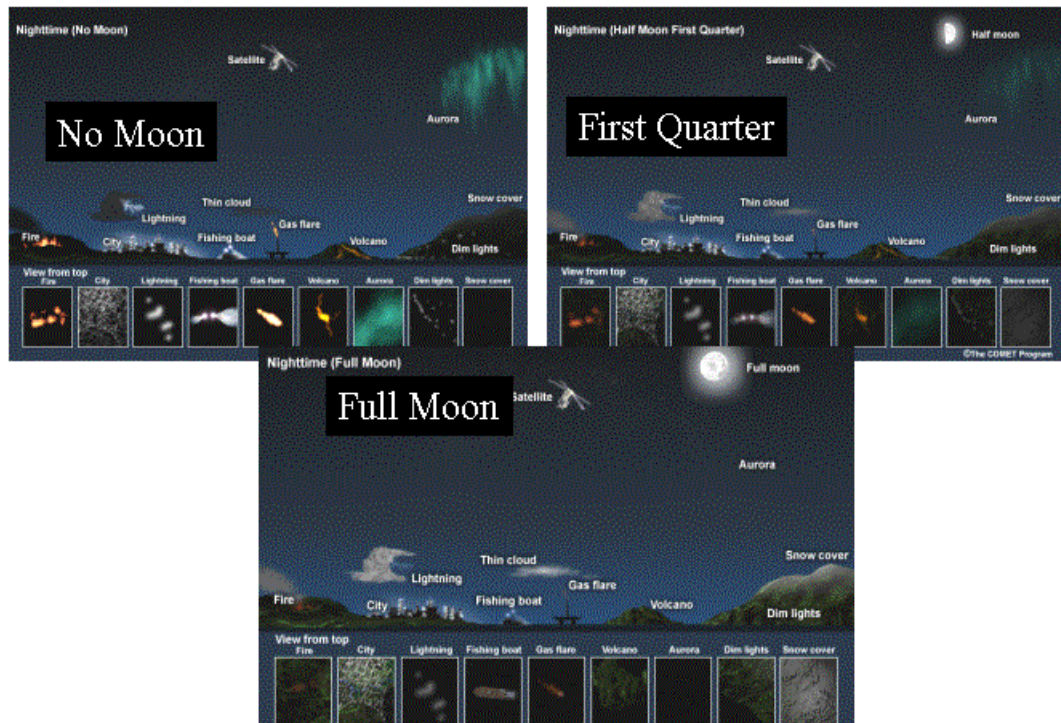


Fig. 7 Example schematics illustrating the change in appearance for various elements of a nighttime visible image as a function of the lunar illumination.

Part of the problem is that these images change appearance significantly based on the level of lunar illumination. In periods of little or no moon (Fig. 7) only self-contained light sources can be seen, including fires, city lights, lightning, the aurora, volcanoes, intensely-lit fishing boats, and natural gas flares. In conditions of quarter moon or more, reflective features start to appear: low clouds, dust plumes, land properties, snow cover, and sea ice (Fig. 7). At full moon (Fig. 7) reflection is maximized, and less gain is needed. Thus, self-contained light sources are dimmer, and clouds appear distinctly.

## 7. Summary and Conclusions

The history of satellite remote sensing is replete with applications that arise when new data sets become available. Here we outlined a few that arose with the advent of the nighttime OLS. However, equipped with knowledge of the engineering and data specifications of the DNB, we made some reasonable assessments about what will be

possible using the OLS. Our hope is that this effort will spur planning and research in the interim before VIIRS DNB data streams become available later in this decade.

## 8. Acknowledgements

The support of the research sponsors, the Oceanographer of the Navy through the Operational Effects Program office (PMW-150) under program element PE-0603207N, the Office of Naval Research under program element PE-0602435N, and the National Polar-orbiting Operational Environmental Satellite System's (NPOESS) Integrated Program Office (IPO) located in Silver Spring, MD, is gratefully acknowledged.

## References

Croft, T.A., 1978. Night-time Images of the Earth From Space. *Scientific American*, 239, 86-98.

Elvidge, C. D., H.W. Kroehl, E.A. Kihn, K.E. Baugh, E.R. Davis, and W.M. Hao, 1996. Algorithm for the Retrieval of Fire Pixels from DMSP Operational Linescan System Data. *Biomass Burning and Global Change: Remote Sensing, Modeling and Inventory Development, and Biomass Burning in Africa*. J. S. Levine. Cambridge, MIT Press, 73-85.

Elvidge, C.D., K.E. Baugh, E.A. Kihn, H.W. Kroehl, E.R. Davis, 1997. Mapping of City Lights Using DMSP Operational Linescan System Data. *Photogrammetric Engineering and Remote Sensing*, 63, 727-734.

Elvidge, C.D., D.W. Pack, E. Prins, E.A. Kihn, J. Kendall, and K.E. Baugh, 1998a. Wildfire Detection with Meteorological Satellite Data: Results from New Mexico during June of 1996 using GOES, AVHRR and DMSP-OLS. *Remote Sensing Change Detection: Environmental Monitoring Methods and Applications*. Ann Arbor Press, 103-121.

Elvidge, C.D., K.E. Baugh, V.R. Hobson, E.A. Kihn, and H.W. Kroehl, 1998b. Detection of Fires and Power Outages using DMSP-OLS data. *Remote Sensing Change Detection: Environmental Monitoring Methods and Applications*. Ann Arbor Press, 123-135.

Foster, J.L., 1983. Nighttime observations of snow using visible imagery. *International Journal of Remote Sensing*, 4, 785-791.

Foster, J.L., and D.K. Hall, 1991. Observations of snow and ice features during the polar winter using moonlight as a source of illumination. *Remote Sensing of the Environment*, 37, 77-88.

Fuller, D. O. and M. Fulk, 2000. Comparison of NOAA AVHRR and DMSP-OLS for operational fire monitoring in Kalimantan, Indonesia, *International Journal of Remote Sensing*, 21, 181-187.

Johnson, D.B., P. Flament, and R.L. Bernstein, 1994, High Resolution Satellite Imagery for Mesoscale Meteorological Studies, *Bull. Amer. Met. Soc.*, 75, 5-33.

Orville, Richard E., 1981: Global Distribution of Midnight Lightning--September to November 1977. *Monthly Weather Review*, 109, 391-395.

Orville, Richard E., and R.W. Henderson, 1986. Global Distribution of Midnight Lightning: September 1977 to August 1978, *Monthly Weather Review*, 114, 2640-2653.

Sullivan, W.T. III, 1989. A 10 km Resolution Image of the Entire Night-time Earth Based on Cloud-free Satellite Photographs in the 400-1100 nm Band. *International Journal of Remote Sensing*, 10, 1-5.